Received: 17 June 2019 | Revised: 2 October 2019 | Accepted: 3 October 2019

DOI: 10.1002/nbm.4203

RESEARCH ARTICLE

WILEY NMR IN BIOMEDICINE

Detection of cortical malformations using enhanced synthetic contrast images derived from quantitative T1 maps

Ulrike Nöth[1] | René-Maxime Gracien[2] | Michelle Maiworm[3] | Philipp S. Reif[2,4] | Elke Hattingen[3] | Susanne Knake[5] | Marlies Wagner[3] | Ralf Deichmann[1]

[1] Brain Imaging Center, Goethe University, Frankfurt am Main, Germany

[2] Department of Neurology, Goethe University, Frankfurt am Main, Germany

[3] Institute of Neuroradiology, Goethe University, Frankfurt am Main, Germany

[4] Epilepsy Center Frankfurt Rhine-Main, Goethe University, Frankfurt am Main, Germany

[5] Epilepsy Center Hessen, University Hospital Marburg, Marburg, Germany

Correspondence
Dr. Ulrike Nöth, Goethe University, Brain Imaging Center (BIC), Schleusenweg 2-16, 60528. Frankfurt am Main, Germany.
Email: noeth@med.uni-frankfurt.de

Funding information
LOEWE-Program "Center for Personalized Translational Epilepsy Research" (CePTER) of the Land Hessen, Germany, Grant/Award Number: Aktenzeichen: 519/03/03.001

The detection of cortical malformations in conventional MR images can be challenging. Prominent examples are focal cortical dysplasias (FCD), the most common cause of drug-resistant focal epilepsy. The two main MRI hallmarks of cortical malformations are increased cortical thickness and blurring of the gray (GM) and white matter (WM) junction. The purpose of this study was to derive synthetic anatomies from quantitative T1 maps for the improved display of the above imaging characteristics in individual patients.

On the basis of a T1 map, a mask comprising pixels with T1 values characteristic for GM is created from which the local cortical extent (CE) is determined. The local smoothness (SM) of the GM-WM junctions is derived from the T1 gradient. For display of cortical malformations, the resulting CE and SM maps serve to enhance local intensities in synthetic double inversion recovery (DIR) images calculated from the T1 map.

The resulting CE- and/or SM-enhanced DIR images appear hyperintense at the site of cortical malformations, thus facilitating FCD detection in epilepsy patients. However, false positives may arise in areas with naturally elevated CE and/or SM, such as large GM structures and perivascular spaces.

In summary, the proposed method facilitates the detection of cortical abnormalities such as cortical thickening and blurring of the GM-WM junction which are typical FCD markers. Still, subject motion artifacts, perivascular spaces, and large normal GM structures may also yield signal hyperintensity in the enhanced synthetic DIR images, requiring careful comparison with clinical MR images by an experienced neuroradiologist to exclude false positives.

KEYWORDS

cortical malformation, cortical thickness, double inversion recovery (DIR), focal cortical dysplasia (FCD), gray-white matter blurring, quantitative T1 mapping

Abbreviations: B1, RF transmit field; BW, receiver band width; cc, correlation coefficient; CE, cortical extent; CSF, cerebrospinal fluid; D, shortest distance to the edge of the GM mask; DIR, double inversion recovery; EP, enhancement parameter; FCD, focal cortical dysplasia; FLAIR, fluid attenuated inversion recovery; GE, gradient echo; GM, gray matter; GMC, gray matter characteristics; MAP, Morphometric Analysis Programme; MPRAGE, magnetization prepared rapid acquisition of gradient echoes; PD, proton density; qMRI, quantitative MRI; RF, radio frequency; ROI, region of interest; RP, receive profile; SL, sensitivity level; SM, smoothness; TM, tissue mask; VFA, variable flip angle; WM, white matter; α, excitation angle

1 | INTRODUCTION

Quantitative MRI (qMRI) techniques do not only allow for the direct measurement of certain tissue parameters such as the longitudinal relaxation time T1 in pathologic tissue[1,2] but have also been useful for enhancing pathology specific tissue characteristics, thus improving the visual assessment of certain brain pathologies.[3,4] The question arises whether qMRI data can also be used to derive MR images with special contrasts for improved visualization of focal cortical malformations which can be difficult to detect in conventional MR images. A prominent example of cortical malformations with cytoarchitectural and frequently also neuronal abnormalities[5,6] are focal cortical dysplasias (FCD), a common cause of drug-resistant focal epilepsy. In these patients, surgery might be a treatment option, requiring accurate FCD detection.

Previous study results revealed that 60–91% of FCDs showed cortical thickening and 74–96% blurring of the junction between grey (GM) and white matter (WM),[7,8] which thus seem to be the two most promising parameters for detecting a majority of FCDs. Furthermore, alterations in WM signal near the cortex may resemble an estuary that extends funnel-shaped towards the ventricle, reflecting the involvement of radial glialneuronal units (transmantle sign).[9,10]

Various techniques for FCD detection have been proposed, which differ in MRI data acquisition, data segmentation, calculation of cortical thickness, quantification of GM-WM blurring, and data display, as discussed in the following sections.

For MRI data acquisition, T1-weighted sequences with 1 mm isotropic resolution are frequently used to achieve a distinct GM-WM contrast.[8,11-14] Furthermore, the double inversion recovery (DIR) sequence which suppresses simultaneously signal from WM and cerebrospinal fluid (CSF)[15] has been successfully used for FCD detection with a spatial resolution of 1x1x2 mm[3.16]

Data segmentation usually requires a signal non-uniformity correction.[11,12,17] Alternatively, the MP2RAGE sequence[18] which provides a structural data set that is free from the receive profile (RP) bias, less affected by inhomogeneities of the radio frequency (RF) transmit field (B1) and purely T1-weighted, has been successfully applied for FCD detection.[19]

For calculation of the cortical thickness, several algorithms have been proposed[13] which are in general either surface-based[20,21] or voxel-based.[8,11,22]

Similarly, several algorithms are available for estimation of GM-WM blurring,[13] employing different concepts: calculation of the absolute gradient of signal intensities across the GM-WM junction,[8,11] calculation of the boundary thickness,[23] quantification of the contrast between WM and GM close to the junction,[21] or calculation of junction images that show voxels which cannot be clearly attributed to either WM or GM.[12]

For the display of the parameters indicating GM thickening and/or GM-WM blurring in a way that allows for the detection of abnormal values, there are mainly two techniques. The first technique is based on an individual brain analysis, so FCDs have a different intensity than surrounding normal tissue. As an example, FCDs appear hyperintense in ratio maps which are defined as the product of cortical thickness and image signal divided by the GM gradient.[11] The second technique compares individual patient data with a large cohort of normal controls.[12,14,16,21] The Morphometric Analysis Programme (MAP), frequently used in the clinical setting, applies this concept[12] and has been shown to significantly increase the diagnostic sensitivity for FCD type II.[14]

Standard FCD detection using conventional clinical MRI data such as DIR or fluid attenuated inversion recovery (FLAIR) images requires visual exploration of the GM-WM junction to find subtle abnormalities in the morphological appearance and/or in local signal levels. This conventional approach has certain limitations: there is a high demand on the uniformity of signal levels and contrasts in the underlying conventional MRI data and on the experience and attention of the radiologist to spot subtle cortical malformations. Automated or semi-automated techniques as described above reduce the subjective factor by enhancing subtle changes in the GM-WM transition zone. However, the success of FCD detection still depends on the uniformity of signal contrasts and signal levels across the MR images. Furthermore, most methods are based on the second display technique described above, highlighting local deviations from normal values measured on a healthy subject cohort, thus requiring image normalization to a standard template.

The method proposed here is based on quantitative T1 maps acquired with qMRI techniques. In contrast to conventional MRI data, quantitative relaxation time maps provide physically meaningful values (in this case T1, given in ms), rather than just signal levels. This approach has several advantages: (1) Quantitative parameter maps are intrinsically corrected for any spatial signal bias imposed by non-uniformities of the RF coil sensitivity profiles, facilitating the derivation of tissue masks. (2) Quantitative values are ideally independent of the scanner software and hardware (albeit not the field strength), and in fact an increased inter-site reproducibility has been reported for qMRI maps, as compared to conventional data.[24] (3) The proposed method does not require data normalization as it is based on the first display technique described above, enhancing areas where evaluated parameter values differ from those of surrounding normal tissue.

In summary, the presented method highlights areas of focal cortical thickening and areas with blurring of the GM-WM junction by deriving two parameters from quantitative T1 maps with 1 mm isotropic resolution: the local cortical extent (CE) which follows from the distance of a GM voxel from the surface of the surrounding compact GM structure and the smoothness (SM) of the GM-WM junction which is derived from local T1 gradients and their standard deviation across the junction. Signal enhancement is performed if CE and SM exceed normal variations, so cortical malformations appear hyperintense as compared to surrounding normal brain regions. Synthetic DIR data were derived from the T1 maps and used as underlying MR image for signal enhancement. The method was tested on healthy controls, epilepsy patients with FCDs and a patient with tuberous sclerosis.

2 | MATERIALS AND METHODS

2.1 | Subjects

The study was approved by the local ethics committee, and all participants gave written informed consent before participation.

This prospective technical study for the development of a method that facilitates the detection of cortical malformations is part of a more comprehensive clinical study, employing multi-parametric qMRI for quantitative comparison of tissue parameters in epilepsy patients and healthy volunteers.

The method described below was developed on the basis of qMRI data acquired on the first consecutive 8 patients (5 m, 3 f; age range: 19–55 years; mean: 31.5 years) included in this ongoing clinical study, who fulfilled the following inclusion criteria: (1) minimum age of 18 years, (2) diagnosis of epilepsy based on clinical criteria, and (3) diagnosis of FCD based on visual inspection of clinically indicated 3 T MRI images optimized for epilepsy diagnostics.[25] The latter was performed by a senior neuroradiologist experienced in imaging of epilepsy. In addition, the method was tested on a patient with tuberous sclerosis (f, 25 years), since tubera typically share histopathological features of some types of FCD. For comparison, the method was also tested on the first consecutive 5 healthy control subjects included in the study (2 m, 3 f; age range: 19–64 years; mean: 30 years, no history of neurological or psychiatric disorders).

After inclusion in the study, all participants underwent the qMRI protocol as described below.

2.2 | Acquisition of MR data

All research scans were performed on a 3 T whole body MR scanner (Magnetom TRIO, Siemens Medical Solutions, Erlangen, Germany), with a body coil for RF transmission and an 8-channel phased-array head coil for signal reception.

Quantitative T1 maps were acquired via the variable flip angle (VFA) technique which is based on the acquisition of spoiled gradient echo (GE) images with different excitation angles (α), thus modifying image contrasts since GE data acquired with low or high α display proton density (PD) or T1 weighting, respectively. Thus, T1 can be calculated from the contrast differences, as described in the literature.[26,27] In the protocol used, two 3D GE data sets were acquired with the following imaging parameters: FOV = 256x224x160 mm^3, matrix size 256x224x160, TR/TE = 16.4 ms/6.7 ms, α_1/α_2 = 4°/24°, receiver bandwidth (BW) 222 Hz/Pixel. A FLASH-EPI hybrid readout was used to improve the SNR.[28] The acquisition time was 4:54 min per data set, i.e. 9:48 min in total. Non-uniformities of B1 were measured as described by Volz.[29] In summary, this technique acquires two GE data sets, one of which is magnetization prepared via an RF pulse which reduces the longitudinal magnetization and thus the image intensity. Thus, from the quotient of the two data sets the actual preparation angle can be determined and B1 follows from comparison with the nominal value. The same FOV as for T1 mapping with identical volume coverage and a matrix size of 64x56x40 was used, yielding an isotropic spatial resolution of 4 mm. The other parameters were: TR/TE = 11 ms/5 ms, α = 11°, BW = 260 Hz/Pixel. The acquisition time was 53 s.

FLAIR data sets were acquired as part of the research protocol for defining regions of interest (ROI) inside the FCD for quantitative analysis. The parameters were: FoV = 256x220x160 mm^3, matrix size = 256 x 220 x 160, TR/TE/TI = 5000/353/1800 ms, BW = 930 Hz/pixel, and duration 7:12 min.

2.3 | Data processing

Brain extraction was performed with the software tool "bet" from the FMRIB Software Library (FSL, http://www.fmrib.ox.ac.uk/fsl). All other calculations were performed with custom-built programs written in MatLab (MathWorks, Natick, MA). For comparison, data segmentation was performed with the recon-all stream implemented in FreeSurfer (Athinoula A. Martinos Center for Biomedical Imaging, Boston, MA, USA).

Calculation of CE and SM of WM-GM junctions in general requires data segmentation into WM and GM masks. However, most automatic segmentation algorithms utilize information on normal brain architecture. This bears the risk that minor cortical malformations remain undetected due to insufficient segmentation reliability in cases of differences between the target anatomy and the norm.[30] As a consequence, the use of manual and semiautomatic segmentation tools has been proposed for these cases.[30] To avoid potential problems, the method presented here does not employ standard data segmentation but rather calculates GM characteristics (GMC) masks comprising all pixels with T1 values that are typical for GM. It has been shown in the literature that approximate T1 ranges at 3 Tesla are 650 to 1050 ms for WM and 1200 to 1600 ms for GM.[31] For the whole data evaluation procedure described below, the following six input parameters are used to initiate the tissue classification procedure: T1 min(WM) = 650 ms, T1max(WM) = 1050 ms, T1 min(GM) = 1200 ms, T1max(GM) = 1600 ms. Furthermore, for recognizing small WM or CSF structures enclosed inside GM it is assumed that the minimum T1 difference between these structures and the surrounding GM is ΔT1 (WM) = 100 ms and ΔT1(CSF) = 100 ms. Please note that these values are considerably smaller than normal T1 differences between WM and GM or CSF and GM, to account for partial volume effects.

2.3.1 | T1 based calculation of GM characteristics (GMC) masks

A tissue mask (TM) is created by skull-stripping the high angle VFA data set using "bet" and excluding all pixels with T1 < T1 min(WM). For compactness, small enclosed areas in TM with a value of zero are filled. All further data processing is restricted to pixels inside TM.

The median T1 value median(T1) and the standard deviation std(T1) is calculated across all pixels with a T1 value between T1 min(WM) and T1max(WM). For each pixel inside TM, a value K is determined as K = (T1-median(T1))/std(T1). Thus, large values of K denote pixels with T1 values that are considerably longer than the median T1 in bulk WM which increases the likelihood that they belong to GM. Pixels with K > 4 are attributed to a bulk GMC mask. Furthermore, pixels with $2 < K \leq 4$ are added to this mask, provided they are connected. This is performed via a mask growing algorithm, using the bulk GMC mask as a seed mask and adding recursively adjacent pixels (i.e. pixels inside an outer 1 pixel shell), provided they have a K-value between 2 and 4. Pixels with T1 > 1.5*T1max(GM) are then removed from the GMC mask and attributed to CSF.

As an example, Figure 1 shows for a healthy subject a single slice of the T1 map (left), an enlarged frontal region (Figure 1a) and the result of the initial tissue classification (Figure 1b), indicating the GMC start mask (red) and the start masks with pixels classified as WM (green) and CSF (blue). For large homogeneous areas in the T1 map, each tissue type is attributed correctly. However, problems arise for small areas due to partial volume effects: small CSF compartments enclosed in GM structures (white arrows) (such as CSF in the sulci) and small WM compartments enclosed in GM structures (grey arrows) are frequently misinterpreted as GM.

For improvement of results, local T1 maxima and minima with a sufficiently marked ΔT1 are identified inside the GMC start mask, attributing the maxima to CSF and the minima to WM. For this purpose, the T1 gradient **G** is calculated, pointing from short to long T1 values, i.e. from WM across GM to CSF (see Figure 2a, arrows). For calculation of a T1 gradient component in a certain spatial direction, an "upper" and a "lower" gradient, $G^{(+)}$ and $G^{(-)}$, are calculated for a pixel with number i via $G^{(+)}(i) = T1(i + 1)\text{-}T1(i)$ and $G^{(-)}(i) = T1(i)\text{-}T1(i\text{-}1)$ and averaged. In cases where one of the gradients cannot be calculated because one of the contributing pixels is outside TM, only the respective other gradient is used. Subsequently, the maps $|\langle \mathbf{G} \rangle|$ and $\langle |\mathbf{G}| \rangle$ are derived where the brackets represent spatial averaging across nearest neighbors (via convolution with a cubic 3x3x3 pixel kernel) and the vertical bars signify calculation of the vector length. Furthermore, an "enhancement parameter" (EP) is calculated voxel-wise according to:

$$EP = 1 - \frac{|\langle \mathbf{G} \rangle|}{\langle |\mathbf{G}| \rangle} \tag{1}$$

In areas where **G** is homogeneous (enclosed by dotted lines in Figure 2), $|\langle \mathbf{G} \rangle|$ and $\langle |\mathbf{G}| \rangle$ yield identical values, so EP = 0 (Figure 2b). In small enclosed CSF (black line) or WM (white line) structures, **G** changes polarity, so $|\langle \mathbf{G} \rangle|$ is zero and EP = 1 (Figure 2b). Thus, the EP map highlights small enclosed WM and CSF structures. For the creation of an EP mask, a threshold has to be applied. The problem with a fixed threshold is the fact that maximum EP values inside enclosed CSF or WM structures are variable (see Figure 2b): the choice of a higher threshold risks to exclude areas with smaller maximum EP values, whereas a lower threshold yields variable widths of enclosed CSF or WM structures in the EP mask (i.e.

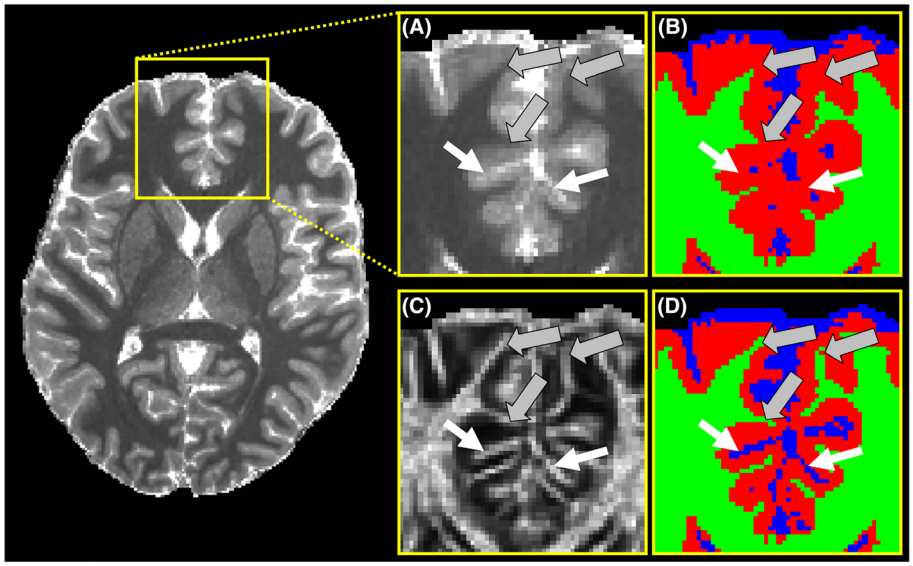

FIGURE 1 Data for a healthy subject: (left) T1 map, (a) enlarged frontal area of the T1 map, (b) start tissue masks for WM (green), GM (red) and CSF (blue), (c) enhancement parameter (EP) map, and (d) final tissue masks. Grey/white arrows indicate small WM/CSF structures surrounded by GM, which are recognized in the final tissue masks, but not in the start masks

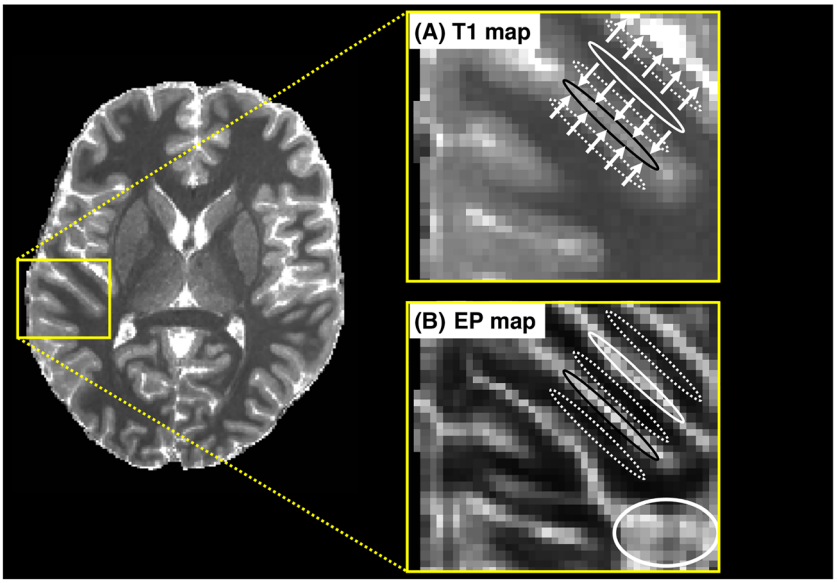

FIGURE 2 Data for a healthy subject: (left) T1 map, (a) enlarged lateral area of the T1 map, (b) map of the enhancement parameter EP. The T1 gradient (arrows) points from short to long T1 values. EP has low values in areas where the T1 gradient is homogeneous (dotted lines) and high values in small areas of enclosed CSF (black line) or WM (white line). In areas with a local maximum or minimum of T1, as in some WM areas, EP will also assume high values (white circle)

larger widths for areas with higher EP values). For improved results, two thresholds are applied, a relatively low fixed threshold of 0.25 for excluding small EP values and a variable threshold chosen as follows: for each pixel, the minimum and maximum EP value across nearest neighbors (i.e. inside a cubic 3x3x3 pixel kernel) are determined and the pixel is included in the EP mask if its EP value exceeds the average of these two values. This procedure makes the widths of enclosed WM or CSF structures independent of the local maximum EP value.

To distinguish between local T1 maxima (CSF) and minima (WM), T1 and EP data are collected across nearest neighbors, i.e. across 3x3x3 pixel areas, and a linear fit is performed according to:

$$T1 = p0 + p1 \cdot EP \tag{2}$$

The correlation coefficient (cc) of the linear fit is also determined. For small enclosed CSF/WM structures inside GM, T1 increases/decreases with EP, so p1 and cc must be positive/negative. Furthermore, to guarantee sufficient salience of the maxima and minima, the parameter V = EP*abs(p1) is calculated and a lower threshold corresponding to ΔT1(CSF) and ΔT1(WM) is assumed for CSF and WM, respectively: since p1 = ΔT1/ΔEP, V can be written as V = abs (ΔT1)*EP/ΔEP, so assuming that EP and ΔEP are approximately 0.5 near enclosed structures, the lower threshold for V is given by ΔT1(CSF) or ΔT1(WM), respectively.

Therefore, WM and CSF candidates are determined on the following basis:

CSF candidates: inside EP mask, p1 > 0, cc > 0, V > ΔT1(CSF).

WM candidates: inside EP mask, p1 < 0, cc < 0, V > ΔT1(WM).

All WM/CSF candidates for which T1 is at least 10% lower/higher than the local average T1 of GM are added to the WM and CSF start masks with exactly the same mask growing algorithm as described above, using the WM or CSF start mask as seed mask and adding recursively adjacent pixels (i.e. pixels inside an outer 1 pixel shell), provided they form part of the selected WM or CSF candidates. The remaining pixels are attributed to the GMC mask.

Figure 1d shows the resulting final masks which are improved considerably when compared to the start masks (Figure 1b): in particular, small embedded WM (grey arrows) and CSF (white arrows) structures as displayed in the T1 map (Figure 1a) and EP map (Figure 1c) are more reliably recognized.

2.3.2 | Calculation of the smoothness SM of GM-WM junctions

The WM/GM junction is subdivided into three layers: L1 (inside GM, adjacent to WM), L2 (inside WM, adjacent to GM) and L3 (inside WM, adjacent to L2). The absolute T1 gradient (G) is determined inside these layers, mean values av(G) and standard deviations std(G) are calculated across nearest neighbors, i.e. inside 3x3x3 pixel areas, and the parameter P = av(G)*std(G) is determined. For smooth WM/GM junctions, G will be relatively small and uniform across the three layers, yielding low values of av(G) and std(G) and thus of P, so 1/P indicates the degree of smoothness. P is averaged across nearest neighbors, i.e. across 3x3x3 pixel areas, yielding the values P_{av} which are only considered inside the central layer L2. SM is calculated according to:

$$SM = \frac{median(P_{av})}{P_{av}} \tag{3}$$

In this equation, the numerator represents the median value of P_{av} in L2 across the whole brain and serves for normalization purposes. As P_{av} appears in the denominator of Equation [3], there is the risk of strong outliers for small P_{av} values. As the analysis of in vivo data shows that the standard deviation of SM inside L2 is about 1.5, SM values are restricted to a maximum of 10, i.e. to the median value plus six standard deviations, reducing the risk that physiologically meaningful values are capped. For better visibility of the results, SM is extended from L2 across the GMC mask, attributing to each pixel inside this mask the SM value in L2 which is geometrically closest. Finally, SM is smoothed via averaging across nearest neighbors, i.e. via convolution with a cubic 3x3x3 pixel kernel.

2.3.3 | Calculation of the cortical extent CE of GM structures

The algorithm comprises two steps. In step 1, for each pixel inside the GMC mask, the shortest distance (D) to the edge of the mask is calculated. A maximum distance of 5 mm (corresponding to a maximum thickness of 10 mm which is sufficient for assessing cortical GM) and a resolution of 0.25 mm are assumed, and each distance is rounded to a multiple of 0.25 mm. The resulting "distance map" assumes low values close to the edge of the GMC mask and high values in the middle of extended GM structures, where the maximum value is 50% of the local extent of the cortex.

In step 2, the CE map is calculated from the "distance map": all pixels with the largest possible value of D and pixels in their local environment, i.e. at a distance of less than D, are identified. Twice the value of D is attributed to these pixels as their CE value. This process is then repeated for the next lower D value, omitting the pixels that have already been labeled in the CE map. This process is performed recursively for all D values. Again, CE is smoothed via averaging across nearest neighbors, i.e. via convolution with a cubic 3x3x3 pixel kernel.

2.3.4 | Enhancement of image data for the visualization of cortical malformations

The goal is to enhance signal intensities in an MR image on the basis of a spatially varying parameter P which is either the SM of the GM-WM junction or the local CE, as introduced above. The enhancement should fulfill the following conditions: (1) there should be no enhancement if P is smaller than a lower threshold P_{min}, below which P shows normal fluctuations only. (2) Enhancement should not increase beyond an upper limit P_{max}. To satisfy these conditions, a function f(P) is derived first which assumes values between 0 and 1, according to:

$$f(P) = \frac{P - P_{min}}{P_{max} - P_{min}} \quad \text{for} \quad P_{min} < P < P_{max} \tag{4}$$

with f(P) = 0 for $P \leq P_{min}$ and f(P) = 1 for $P \geq P_{max}$.

An image is then enhanced according to:

$$IMAG_{enhanced} = IMAG + (AF - 1) \cdot IMAG \cdot f(P) \tag{5}$$

Here, the amplification factor AF = 4 was chosen, yielding 4-fold signal enhancement for f(P) = 1. For determination of P_{min}, the brain is subdivided into volumes of 9x9x9 pixels, calculating for each subvolume the average value and standard deviation of P. Median values of av(P) and std(P) across the whole brain are determined and P_{min} follows from P_{min} = median[av(P)] + *SL**median[std(P)]. For larger values of the sensitivity level (*SL*), the threshold P_{min} is relatively high, yielding a low sensitivity as only larger deviations of the parameter P yield signal enhancement. In contrast, the sensitivity can be increased by reducing the value of *SL* and thus P_{min}. For all evaluations, *SL* = 3 is chosen as standard setting and denoted as normal sensitivity. Furthermore, test versions of enhanced images with low (*SL* = 4), elevated (*SL* = 2) and high (*SL* = 1) sensitivity are created for comparison. For P_{max}, the 90th percentile of all P values with $P > P_{min}$ is chosen.

It should be noted that Equation [5] allows for the enhancement of any MR image that is coregistered to the T1 data. However, as the goal of this study was to derive all data from the T1 maps, synthetic images are calculated as described in the next step.

2.3.5 | Calculation of synthetic MPRAGE and DIR data

Two types of synthetic data sets are calculated: synthetic T1-weighted magnetization prepared rapid acquisition of gradient echoes (MPRAGE) data which will serve in the results section for display purposes and for segmentation using FreeSurfer to test the quality of the GMC masks, and synthetic DIR data which will serve as substrate images for enhancement via the parameters CE and SM.

Synthetic T1-weighted MPRAGE data are derived from the T1 maps, using a mathematical algorithm described in the literature[4] with the target parameters TR = 1900 ms, TI = 900 ms, and α = 9°. FOV and spatial resolution are identical to the respective parameters of the T1 map.

For calculation of synthetic DIR data, the following Fermi filter is used:

$$f_{\pm}(x, x_0, \Delta x) = \frac{1}{1 + \exp\left[\pm\frac{\ln(19)}{\Delta x}\cdot(x - x_0)\right]} \tag{6}$$

The positive/negative sign yields a low pass/high pass filter, respectively, x_0 is the cut-off value and Δx is half the filter width, i.e. f(x) changes from 5% to 95% across 2* Δx.

It should be noted that the synthetic DIR data merely serve as substrate images for enhancement via the parameters CE and SM. For this purpose, only the T1 selectivity of conventional DIR images was replicated, yielding a suppression of signal from WM and CSF and an almost exclusive display of GM structures. Other features such as T2-weighting were not included (which would require the additional acquisition of a T2 map). At 3 Tesla, parameters recommended for DIR in the literature[32] are: TR = 10s, TI1 = 3000 ms, TI2 = 510 ms. Calculation of the resulting T1 filter characteristics according to Madhuranthakam et al.[33] shows that it has a maximum at about 1600 ms with suppression of longer and shorter T1 compartments. This was replicated by applying a high pass and a low pass filter to the T1 map:

$$DIR = C\cdot f_{-}(T1,\ \ 1100,\ \ 500)\cdot f_{+}(T1,\ \ 2200,\ \ 700) \tag{7}$$

The resulting DIR is maximized for T1 = 1600 ms where it achieves a value of 1000 via appropriate choice of the scaling constant C. Pixels outside TM are set to zero in DIR. To avoid spurious signal from CSF, a map M1 is obtained by smoothing the CSF mask across nearest neighbours via convolution with a 3x3x3 cubic kernel. Pixels inside the original CSF mask are set to 1 in M1. Thus, the complementary map M2 = 1-M1 assumes values of 0 inside CSF, values between 0 and 1 in a 1-pixel layer around CSF and values of 1 elsewhere. DIR is multiplied with M2, thus removing CSF pixels from DIR and reducing the signal in DIR for pixels directly adjacent to CSF to avoid partial volume effects.

The synthetic DIR data were used as underlying images for enhancement as described above. Two enhanced types of DIR were calculated, using P=SM or P=CE.

To test the dependence of data processing results on the choice of the six input parameters (i.e. the approximate upper and lower T1 limits for WM and GM and the minimum salience of enclosed WM or CSF structures embedded in GM), data processing was repeated twice for each subject, either reducing or increasing all input parameters by 10%. It should be noted that this is a marked change. As an example, a reduction of parameter values by 10% corresponds to the assumption of T1 ranges of 585 to 945 ms for WM and 1080 to 1440 ms for GM, both values being considerably lower than typical 3 Tesla T1 ranges reported in the literature.[31]

2.4 | Analysis of patient data

For a quantitative analysis of patient data, the FLAIR data sets were coregistered to the T1 maps and served for localizing the FCD and defining respective ROIs. For each patient, the site of the FCD in the FLAIR image was verified by visually comparing the FLAIR image with the corresponding clinical MRI data used for initial diagnosis. These data had been acquired at different hospitals, equipped with different hardware and software and using different MRI protocols, usually comprising T1-weighted MPRAGE, T2-weighted FLAIR, T2-weighted turbo spin echo, susceptibility-weighted and diffusion-weighted sequences. ROI placement was performed by a senior neuroradiologist specialized in epilepsy imaging and an experienced neurologist, taking all decisions by consensus. ROIs comprising 2x2x1 voxels were manually placed in the areas identified as FCDs. Control ROIs of identical size were manually placed in the matching region of the contra-lateral hemisphere with special regard to lobe and cortical or subcortical region. For each patient and ROI, mean values and standard deviations were determined from both enhanced DIR datasets. Values from the FCD and control ROIs were compared separately for each subject. Furthermore, a comparison across all subjects was performed via paired t-tests, using a significance threshold of $p = 0.05$.

3 | RESULTS

Comparison of the CE- or SM-enhanced DIR data sets with high (*SL* = 1), elevated (*SL* = 2), normal (*SL* = 3) and low (*SL* = 4) sensitivity showed that in all investigated cases cortical malformations were clearly visible in the enhanced DIR images calculated with normal (*SL* = 3) sensitivity. Thus, all subsequent data evaluations and figures refer to the data calculated with normal sensitivity.

Figure 3 shows data from a healthy subject (row 1) and two epilepsy patients (rows 2 and 3). In each row, the first three images show for three adjacent slices the results of the FreeSurfer segmentation, indicating the GM-WM boundary (blue) and the pial surface (red). Furthermore, the GMC mask is overlaid (yellow). The last image shows the MPRAGE data for the central slice and serves for orientation. The data from the healthy subject (row 1) show that for cortical areas, there is a very close match between the boundaries of the GMC mask and the segmentation results. In addition, the GMC mask also shows non-cortical GM structures such as the caudate nucleus and the thalamus. Furthermore, in some cortical areas the GMC mask extends beyond the segmentation boundary into WM areas (white arrows). However, comparison with neighbouring slices shows

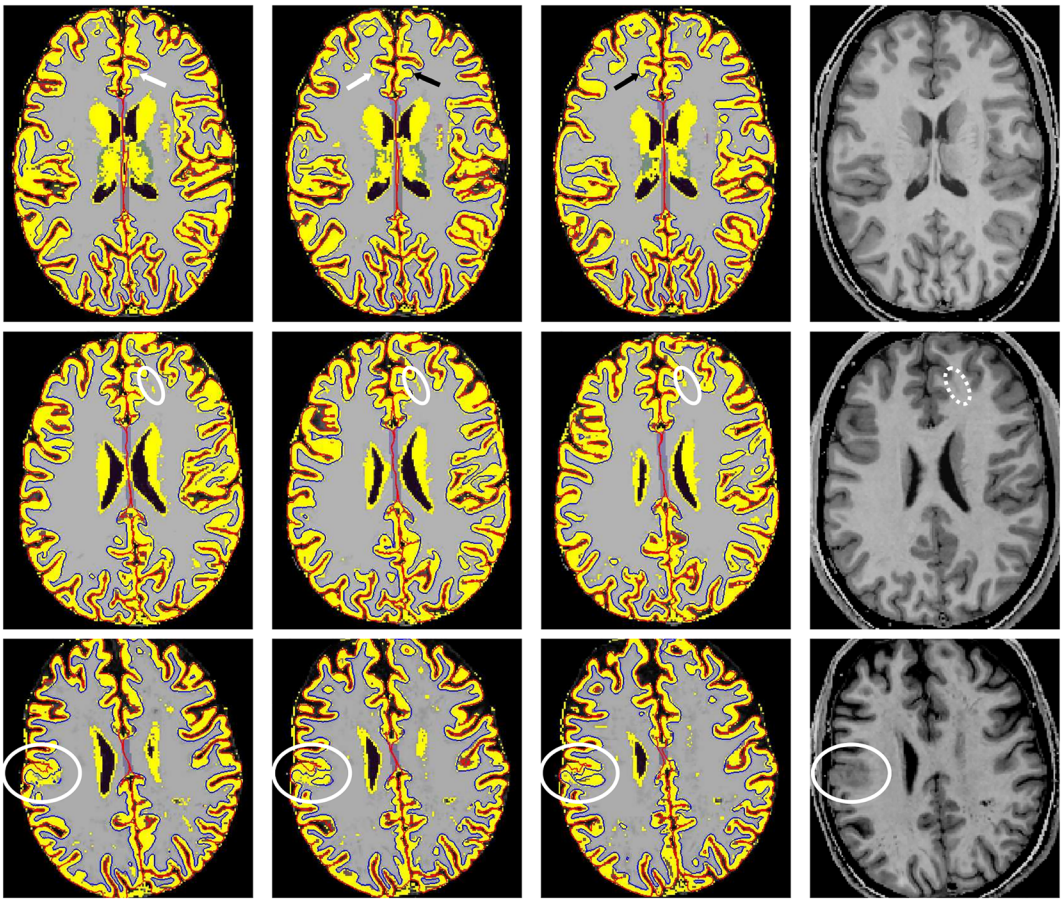

FIGURE 3 Data from a healthy subject (row 1), a patient with a frontal FCD characterized by the transmantle sign (row 2), and a patient with a frontolateral FCD (row 3). Each row shows three adjacent slices of the FreeSurfer segmentation, indicating the WM-GM boundary (blue) and the pial surface (red), with an overlay of the GMC mask (yellow) obtained from the method presented. The MPRAGE image (right) of the central slice is shown for orientation. FCD areas are highlighted by a white ellipse. For the healthy subject (row 1), the GMC mask extends in some places beyond the segmentation boundary into WM areas (white arrows) but is within the boundary in the next slice (black arrows), so the extension beyond this boundary amounts to 1 pixel only

that these areas are adjacent to the GM-WM boundary in the next slice (black arrows), so the extension beyond this boundary amounts to 1 pixel only. The data from the patient in row 2 show a frontal FCD characterized by the transmantle sign (marked by white ellipse). The FCD is included in the GMC mask. In contrast, it is classified as WM by the segmentation. The data from the patient in row 3 show a frontolateral FCD (marked by white ellipse). The FCD and adjoining GM appear as a compact area in the GMC mask. In contrast, the segmentation subdivides the FCD into WM and CSF. In summary, the results demonstrate that the GMC mask shows both actual GM regions and pathologies with T1 values in the GM range.

Figure 4 shows two slices (rows) from a data set obtained on a healthy subject, displaying (from left to right) the T1-weighted MPRAGE, the DIR, the CE- and the SM-enhanced DIR images. In the cortex, the enhanced DIR images show only minor signal increases. In contrast, the CE-enhanced DIR image shows marked hyperintensity for large deep brain GM structures (bottom row) such as the caudate nucleus, the putamen and the thalamus. Similarly, the SM-enhanced DIR image appears hyperintense in areas of the thalamus and the putamen, due to the natural blurring of the GM-WM junction delineating these structures.

Figure 5 shows representative data for three patients (rows) in the same arrangement as in Figure 4. The first patient (row 1; same patient as in Figure 3, row 3) was diagnosed with an FCD in the left frontolateral region on the basis of clinical MRI data showing cortical thickening and blurring of the GM-WM junction. Correspondingly, the FCD is clearly visible in both enhanced DIR images, in addition to displaying a hypointense signal in MPRAGE and a hyperintense signal in DIR. Furthermore, there are some spurious signal enhancements in the right hemisphere due to perivascular spaces (see below for details). The second patient (row 2) was diagnosed with an FCD in the left precentral sulcus which is rather inconspicuous in MPRAGE, DIR and the CE-enhanced DIR. In contrast, the FCD is clearly visible in the SM-enhanced DIR. The third row shows data from the tuberous sclerosis patient with several tubera, displaying similar image characteristics as FCDs in the MPRAGE and DIR data. Importantly, the lesions show marked hyperintensity in both enhanced DIR images.

Table 1 shows the results of the quantitative analysis, listing for each patient (rows) mean values and standard deviations of signal intensities in the CE-enhanced (columns 1 and 2) and SM-enhanced (columns 3 and 4) DIR data sets across the FCD-ROI and the contra-lateral control ROI. For

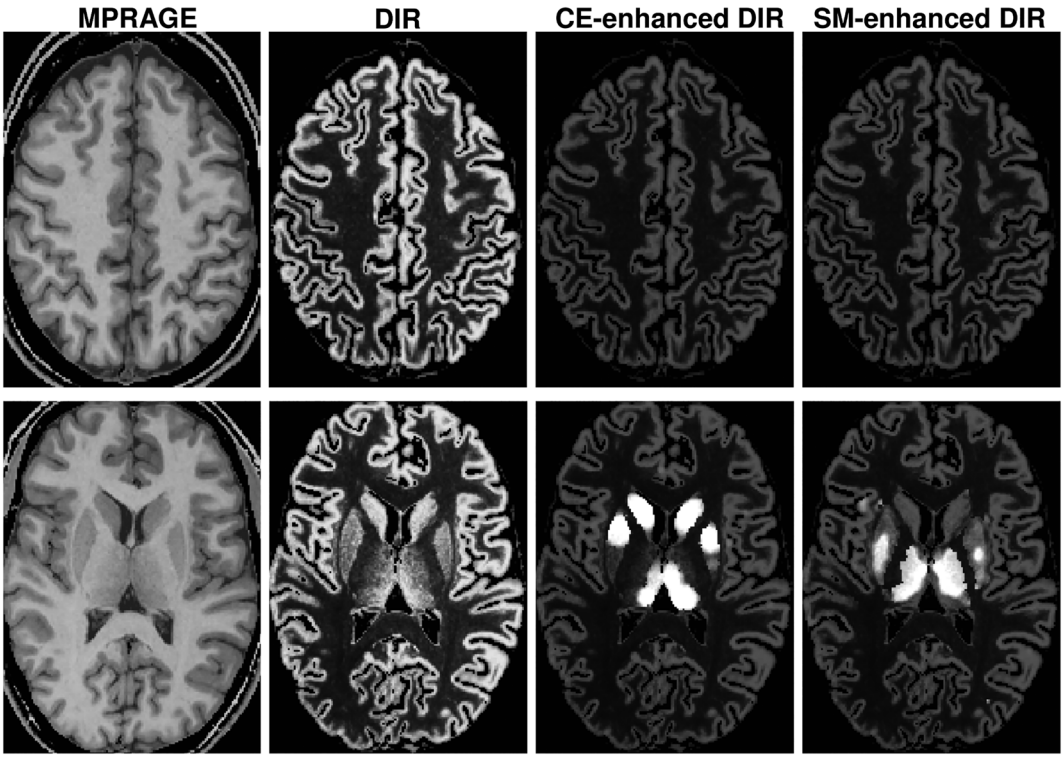

FIGURE 4 Representative data of two different slices (rows) for a healthy subject, showing (from left to right) MPRAGE, DIR, CE- and SM-enhanced DIR images. While cortical areas display only some very minor anterior hyperintensities, GM structures in some deep brain areas show a strong signal hyperintensity in both enhanced DIR images

each case, the enhanced DIR yields higher values in the FCD-ROI than in the control ROI, the difference being more pronounced for the SM-enhanced DIR. On the group level, the intensity difference between FCD and control ROIs was significant for both the CE-enhanced DIR (p = 0.049) and the SM-enhanced DIR (p = 0.011).

Figure 6 shows data from a patient (top row; same patient as in Figure 3, row 2) and a healthy subject (bottom row) in the same arrangement as in Figure 4. The patient suffered from a frontal FCD characterized by the transmantle sign (open arrow) extending from GM into WM, which appears hypointense and hyperintense in MPRAGE and DIR, respectively. This area is not characterized by an increased CE, but clearly visible in the SM-enhanced DIR image due to the smooth signal transition in the T1 data. A similar signal enhancement is caused by perivascular spaces in the deep brain structures. The healthy subject data (bottom row) show an example for a false positive: the SM-enhanced DIR image appears to indicate a transmantle sign (closed arrow). However, the MPRAGE, DIR and CE-enhanced DIR data show no connection of this structure with cortical GM, identifying it as a perivascular space.

Figure 7 shows for a healthy volunteer an example for a false positive caused by subject movement. The top row shows the PD-weighted image (left, only minor subject movement), the T1-weighted image (center, stronger movement) and the quantitative T1 map (right) calculated from the two weighted images. The T1-weighted image shows a signal enhancement in the left and a signal reduction in the right hemisphere. The origin of this artifact is subject motion affecting a certain portion of k-space only, thus leading to a wave-like intensity variation after Fourier transform into image space. Furthermore, spurious residual signal is visible in the background. Thus, the T1 map displays a discrepancy in T1 values between the left and right hemispheres, and a local maximum close to the right cortex as a result of the movement artifact in the T1-weighted image. The bottom row shows from left to right: the MPRAGE, the DIR, the CE-enhanced DIR, and the SM-enhanced DIR images. The latter shows a strong hyperintensity (circle), erroneously suggesting an FCD at the position of the motion-induced apparent T1 enhancement. The experiment was repeated for this subject who remained still during the second measurement. The resulting T1 map and the enhanced DIR data sets were free from artifacts (data not shown), thus confirming that the observed effects were in fact due to subject motion.

Figure 8 shows for four patients (columns) CE-enhanced DIR data sets that were calculated with different input parameters, corresponding to 90% of the standard values (top row), standard values (centre row) and 110% of the standard values (bottom row). The patients shown in column 1–3 correspond to the patients shown in Figure 5, the patient shown in column 4 corresponds to the patient shown in Figure 6 (top). Cortical malformations can be distinguished for all parameter levels (white ellipses). Figure 9 shows the respective result for the SM-enhanced DIR data. Again, cortical malformations can be distinguished for all parameter levels (white ellipses). However, for the reduced input parameter level (top row), there is a stronger occurrence of false positives (white arrows), mainly due to perivascular spaces. The reason is that in this case the assumed

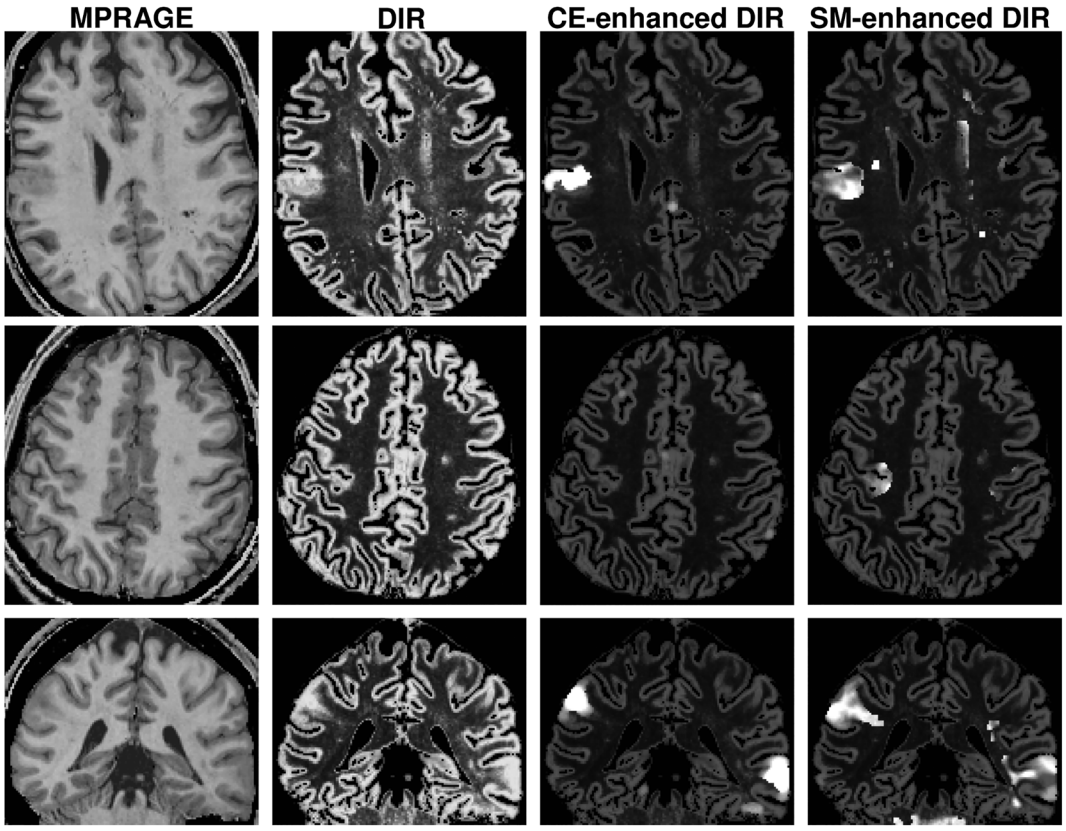

FIGURE 5 Representative data for three patients (rows), arrangement as in Figure 4. The FCD in the left frontolateral region (row 1) appears hyperintense in both enhanced DIR images, whereas the FCD in the left precentral sulcus (row 2) appears hyperintense in the SM-enhanced DIR only. In the patient with tuberous sclerosis (row 3), the two tubera located in the slice shown appear hyperintense in both enhanced DIR images

TABLE 1 Mean value ± SD of signal intensities in FCD and control ROIs for both enhanced DIR images

	CE-enhanced DIR		SM-enhanced DIR	
	FCD ROI	Control ROI	FCD ROI	Control ROI
PAT 1	1327 ± 106	290 ± 74	987 ± 101	290 ± 74
PAT 2	952 ± 35	563 ± 62	983 ± 88	563 ± 62
PAT 3	882 ± 32	711 ± 181	963 ± 114	711 ± 181
PAT 4	452 ± 115	227 ± 32	2270 ± 208	227 ± 32
PAT 5	975 ± 31	649 ± 103	1078 ± 49	801 ± 144
PAT 6	978 ± 23	208 ± 19	1191 ± 198	208 ± 19
PAT 7	2803 ± 108	196 ± 17	997 ± 5	196 ± 17
PAT 8	374 ± 72	302 ± 186	641 ± 150	302 ± 186
Mean ± SD	**1099 ± 758**	**393 ± 212**	**1139 ± 483**	**412 ± 243**

T1 ranges for WM and GM are too low, so WM pixels with slightly increased T1 values are attributed to the GMC mask, yielding more areas labelled as WM-GM boundaries with smooth T1 transitions.

4 | DISCUSSION

The method presented here facilitates the detection of cortical abnormalities such as cortical thickening and blurring of the GM-WM junction (which are typical FCD markers), based on quantitative T1 maps with an isotropic spatial resolution of 1 mm. Cortical thickening is quantified via the parameter CE which is derived from the GMC mask, and blurring of the GM-WM junction is quantified via the parameter SM which follows from the local T1 gradients and their standard deviations across the tissue boundary.

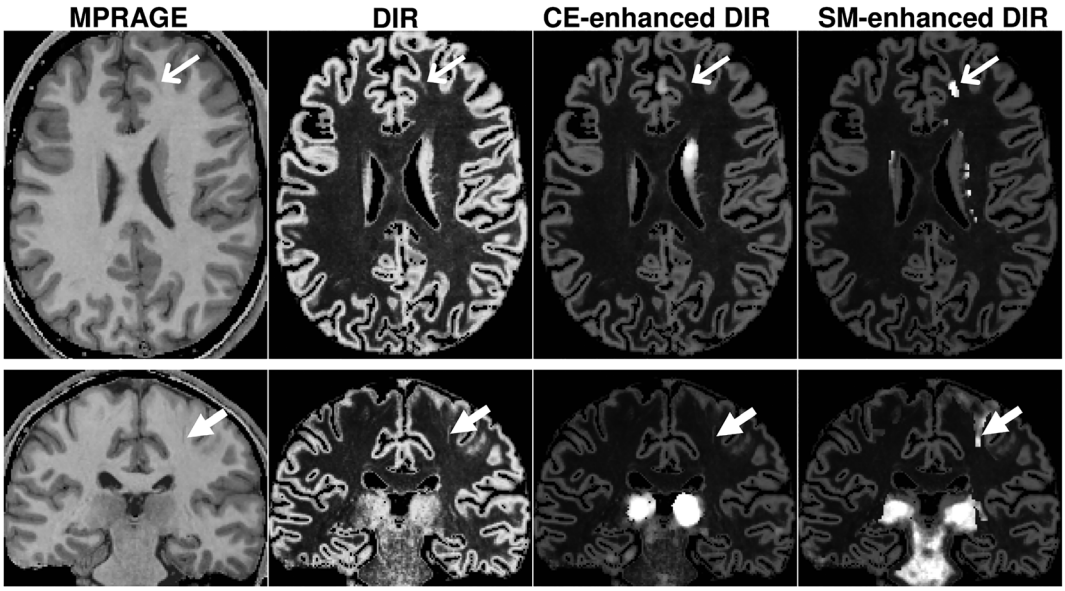

FIGURE 6 Data from a patient (top row) and a healthy subject (bottom row), arrangement as in Figure 4. For the patient, a frontal FCD characterized by the transmantle sign (open arrow) appears hyperintense in the SM-enhanced DIR. The other modalities show that this structure is connected to GM. Further signal enhancement in the SM-enhanced DIR is caused by perivascular spaces in the deep brain structures. For the healthy subject, a perivascular space (closed arrow) displays a hyperintensity in the SM-enhanced DIR similar to a transmantle sign; however, the connection to GM is missing in the other modalities

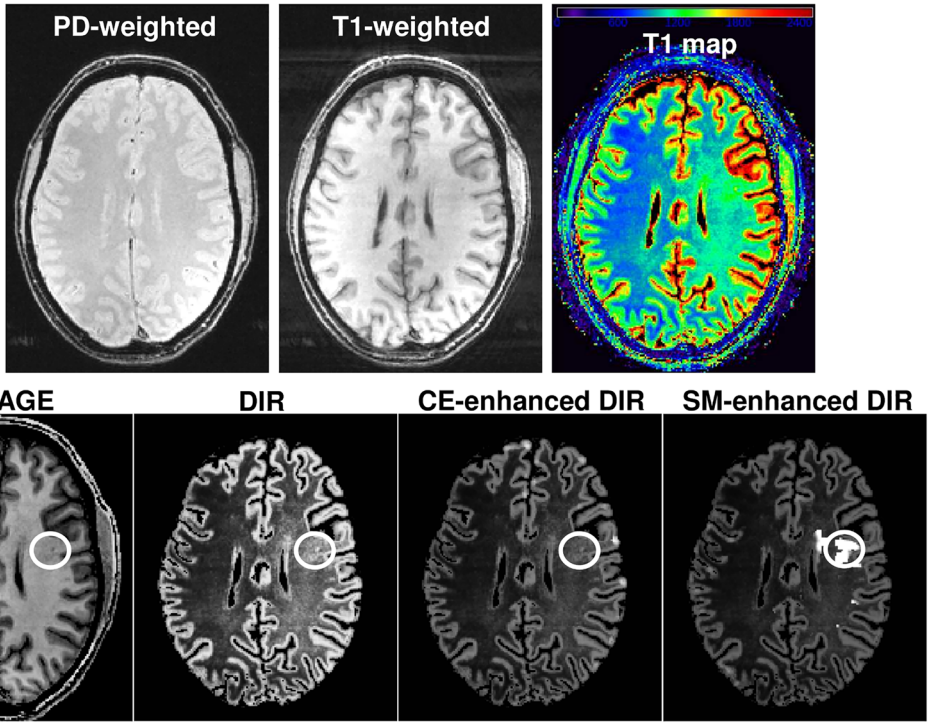

FIGURE 7 False positive caused by subject movement (healthy subject). Top row, from left to right: PD- and T1-weighted image, and resulting T1 map. Bottom row, from left to right: MPRAGE, DIR, CE- and SM-enhanced DIR. The T1-weighted image shows a movement artifact (horizontal stripes in background, signal reduction in right hemisphere), yielding increased T1 values in the right hemisphere and a hyperintensity in the SM-enhanced DIR image, erroneously suggesting an FCD at the site marked with a circle

For displaying the results, synthetic DIR data that show mainly GM structures are derived from the T1 maps. Subsequently, two signal enhanced versions of DIR data are created which appear hyperintense in areas of either increased CE or SM values. A lower limit was imposed on the respective parameter of interest to avoid that minor variations within the normal range yield signal hyperintensity and thus false positives.

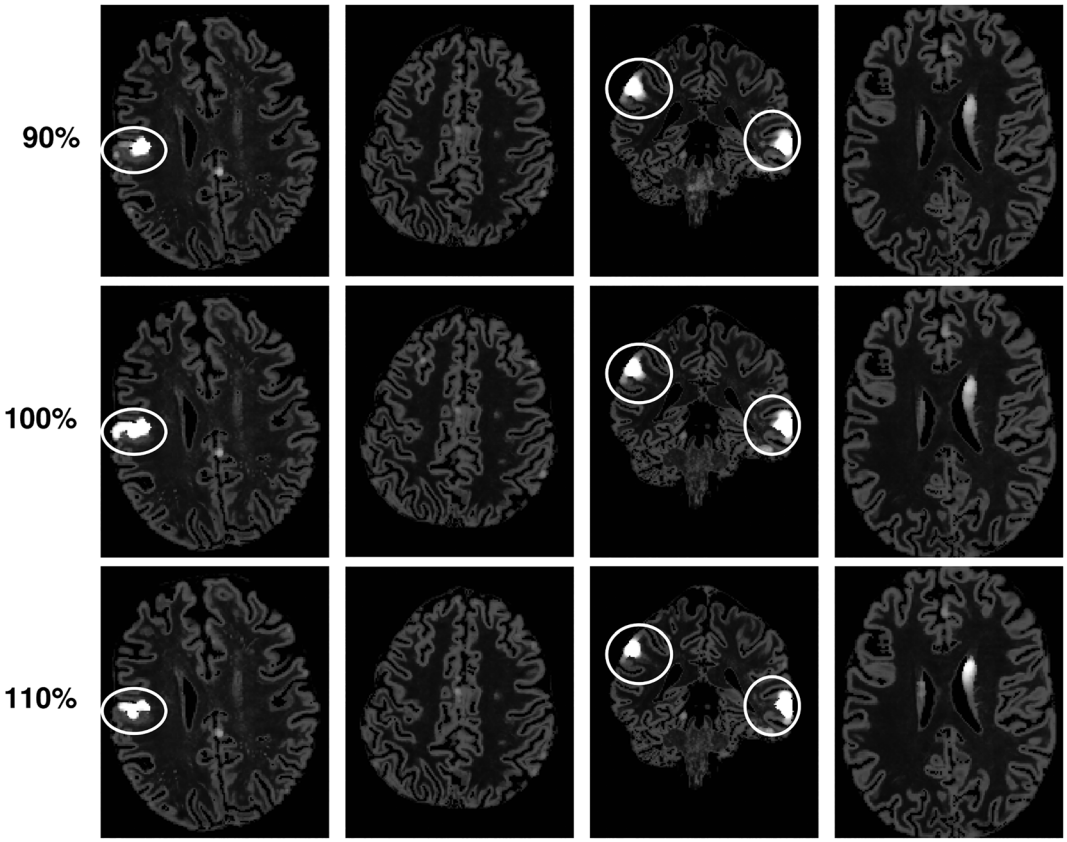

FIGURE 8 CE-enhanced DIR data sets for four patients (columns), calculated with different assumptions of input parameters, corresponding to 90% of the standard values (top row), standard values (Centre row) and 110% of the standard values (bottom row). The patients in column 1–3 correspond to the patients in Figure 5, the patient in column 4 corresponds to the patient in Figure 6 (top). Cortical malformations can be distinguished for all parameter levels (white ellipses)

In contrast to techniques that highlight FCDs by comparing individual patient data to reference data sets acquired on healthy controls,[12] the method presented here provides intrinsic contrasts: FCDs are distinguished via comparison with surrounding normal brain structures, rather than via comparison with healthy controls. Thus, normalization of the data is not required, in contrast to methods that pool data from different subjects.

In a previous publication based on a similar concept,[11] maps of different features (cortical thickness, image signal, gradient of the GM-WM junction) were combined into a single map to increase the hyperintensity and thus the visibility of FCDs. In the method presented here, it was rather chosen to create enhanced DIR data sets separately for each single parameter under investigation, since FCDs do not always show abnormalities in all features simultaneously. Furthermore, these abnormalities may affect different anatomical regions (cortex, GM-WM junction or adjacent WM), so deviations from normal baseline values arising from different features do not necessarily overlap. As an example, CE increases are in general located inside the cortex, whereas SM may be increased around areas of abnormal subcortical GM which, however, do not necessarily yield increased CE values. The differential approach chosen here helps to distinguish between cortical and subcortical abnormalities and reduces the risk that false positives arising from the assessment of the different parameters are combined in a single image.

The concept of distinguishing FCDs via comparison with surrounding normal brain structures provides certain disadvantages, since areas where CE and/or SM are naturally increased will yield false positives. As an example, large GM structures such as the putamen, the thalamus and the amygdalae appear hyperintense in the CE-enhanced DIR. Similarly, perivascular spaces appear hyperintense in the SM-enhanced DIR. Therefore, the user has to be aware of these issues and careful comparison of the enhanced DIR data with standard clinical MRI data is required.

Further problems may arise in the presence of image artifacts. Due to the partial volume effect, small embedded CSF structures may not be recognized correctly during the segmentation process, yielding erroneously high CE values and therefore false positives in the CE-enhanced DIR data. Furthermore, as shown for one case, subject motion artifacts may yield signal reductions in WM which are misinterpreted as blurred embedded GM structures, yielding false positives in the SM-enhanced DIR data.

A further limitation of the proposed method could be that the total acquisition time which is required for quantitative T1 and B1 mapping (ca. 11 min in the current implementation) can be longer than for standard clinical scans.

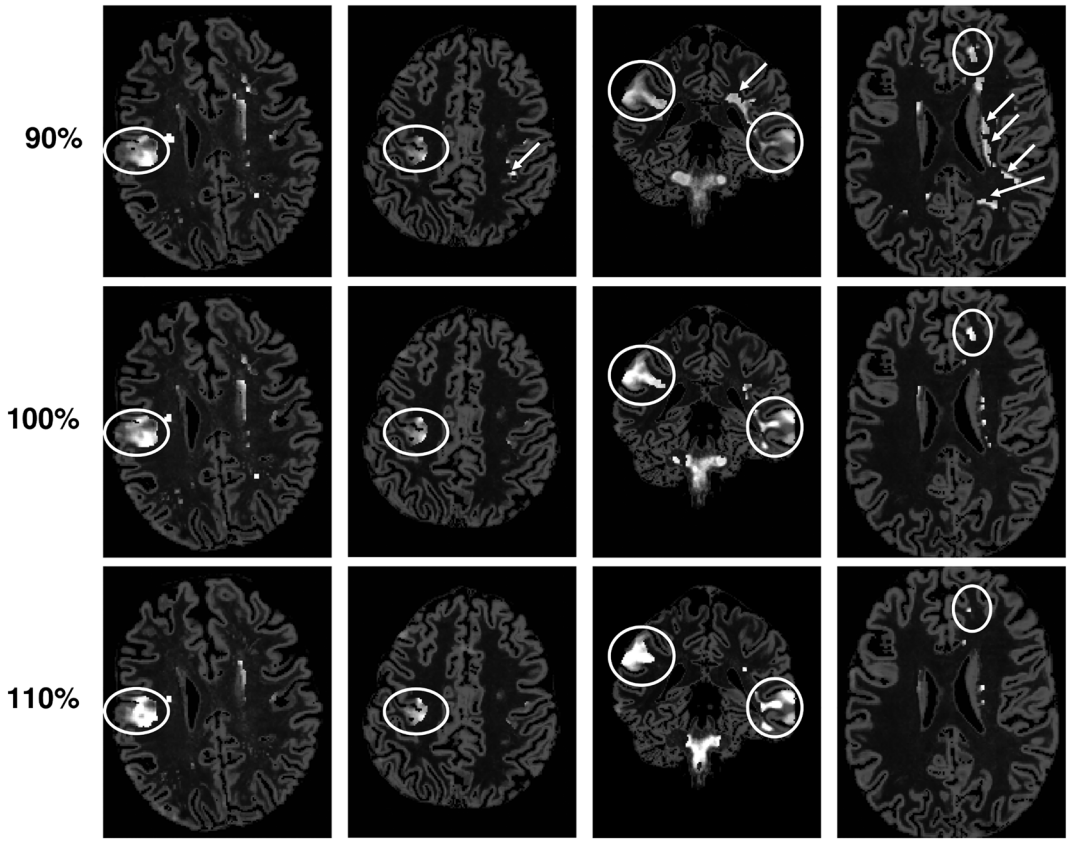

FIGURE 9 SM-enhanced DIR data sets, calculated with different assumptions of input parameters. The arrangement is identical to Figure 8. Cortical malformations can be distinguished for all parameter levels (white ellipses). For the reduced input parameter level (top row), there is a stronger occurrence of false positives (white arrows)

It should also be noted that the T1 prolongation at the site of an FCD is not specific for a certain disease, indicating a focal pathologic process only. As an example, glioma or encephalitis might yield similar patterns in the enhanced DIR data.

There are several ways in which the method might be improved. In the current implementation, only two parameters (SM and CE) were used for signal enhancement. In a previous publication by Bernasconi et al.,[11] it has been proposed to derive a third parameter, dubbed "relative intensity" (RI). In summary, the intensity B_g at the WM-GM boundary is determined, subsequently deriving for each pixel the parameter RI = [B_g - abs (B_g-S)]/B_g where S is the local signal. Inclusion of this additional feature might improve the sensitivity of the method proposed here. Furthermore, it may be advantageous to perform multi-parametric mapping, including other quantitative parameters (such as PD, T2 or diffusion parameters) for improved detection of cortical malformations. The multi-component image series provided by multi-parametric mapping would also allow to use advanced denoising algorithms such as optimized multicomponent nonlocal means combined with principal component analysis[34] or multispectral nonlocal maximum-likelihood filters.[35] Their application to the source data used as input images of the method presented here could lead to further improvements of results.

In summary, the method shows a clear signal enhancement at the site of FCDs which, however, also arises in deep GM structures and perivascular spaces, is not disease specific and may be induced by artifacts. Thus, while these maps alone are not sufficient for a comprehensive analysis of the brain morphology for cortical malformations, they have the advantage of clearly highlighting suspect brain areas, so signal enhancement serves as a marker for potential FCDs. Due to the high contrast in the enhanced maps, suspect areas are easier to identify than in unenhanced maps or standard morphological images. Still, it is required that the identified areas are closely investigated in clinical morphological MR images, such as 3D high-contrast T1-weighted data sets and 3D FLAIR data sets, to confirm if signal enhancement arises from an FCD or an artefact. Therefore, the method should rather be used as a supporting tool by an experienced neuroradiologist, in addition to standard clinical MR images.

FUNDING INFORMATION

This work was supported by the LOEWE-Program "Center for Personalized Translational Epilepsy Research" (CePTER) of the Land Hessen, Germany (Aktenzeichen: 519/03/03.001).

CONFLICT OF INTEREST

PSR reports personal fees from Eisai outside the submitted work.

All other authors report no conflicts of interest relevant to this study.

ORCID

Ulrike Nöth https://orcid.org/0000-0003-0699-4088

René-Maxime Gracien https://orcid.org/0000-0003-1065-940X

REFERENCES

1. Gracien R-M, Jurcoane A, Wagner M, et al. Multimodal quantitative MRI assessment of cortical damage in relapsing-remitting multiple sclerosis. *J Magn Reson Imaging*. 2016;44:1600-1607.
2. Reeves C, Tachrount M, Thomas D, et al. Combined ex vivo 9.4T MRI and quantitative histopathological study in Normal and pathological neocortical resections in focal epilepsy. *Brain Pathol*. 2016;26:319-333.
3. Kober T, Granziera C, Ribes D, et al. MP2RAGE multiple sclerosis magnetic resonance imaging at 3 T. *Invest Radiol*. 2012;47:346-352.
4. Nöth U, Hattingen E, Bähr O, Tichy J, Deichmann R. Improved visibility of brain tumors in synthetic MP-RAGE anatomies with pure T1 weighting. *NMR Biomed*. 2015;28:818-830.
5. Palmini A, Lüders HO. Classification issues in malformations caused by abnormalities of cortical development. *Neurosurg Clin N am*. 2002;13:1-16.
6. Palmini A, Najm I, Avanzini G, et al. Terminology and classification of the cortical dysplasias. *Neurology*. 2004;62:S2-S8.
7. Lerner JT, Salamon N, Hauptman JS, et al. Assessment and surgical outcomes for mild type I and severe type II cortical dysplasia: a critical review and the UCLA experience. *Epilepsia*. 2009;50:1310-1335.
8. Colliot O, Antel SB, Naessens VB, Bernasconi N, Bernasconi A. In vivo profiling of focal cortical dysplasia on high-resolution MRI with computational models. *Epilepsia*. 2006;47:134-142.
9. Urbach H, Scheffler B, Heinrichsmeier T, von Oertzen J, Kral T, Wellmer J, Schramm J, Wiestler OD, Blümcke I. Focal cortical dysplasia of Taylor's balloon cell type: a clinicopathological entity with characteristic neuroimaging and histopathological features, and favorable postsurgical outcome. *Epilepsia* 2002;43:33–40.
10. Colombo N, Tassi L, Deleo F, et al. Focal cortical dysplasia type IIa and IIb: MRI aspects in 118 cases proven by histopathology. *Neuroradiology*. 2012;54:1065-1077.
11. Bernasconi A, Antel SB, Collins DL, et al. Texture analysis and morphological processing of magnetic resonance imaging assist detection of focal cortical dysplasia in extra-temporal partial epilepsy. *Ann Neurol*. 2001;49:770-775.
12. Huppertz H-J, Grimm C, Fauser S, et al. Enhanced visualization of blurred gray-white matter junctions in focal cortical dysplasia by voxel-based 3D MRI analysis. *Epilepsy Res*. 2005;67:35-50.
13. Kini LG, Gee JC, Litt B. Computational analysis in epilepsy neuroimaging: a survey of features and methods. *Neuroimage Clin*. 2016;11:515-529.
14. Wagner J, Weber B, Urbach H, Elger CE, Huppertz H-J. Morphometric MRI analysis improves detection of focal cortical dysplasia type II. *Brain*. 2011;134:2844-2854.
15. Li Q, Zhang Q, Sun H, Zhang Y, Bai R. Double inversion recovery magnetic resonance imaging at 3 T: diagnostic value in hippocampal sclerosis. *J Comput Assist Tomogr*. 2011;35:290-293.
16. Rugg-Gunn FJ, Boulby PA, Symms MR, Barker GJ, Duncan JS. Imaging the neocortex in epilepsy with double inversion recovery imaging. *Neuroimage*. 2006;31:39-50.
17. Ashburner J, Friston KJ. Voxel-based morphometry–the methods. *Neuroimage*. 2000;11:805-821.
18. Marques JP, Kober T, Krueger G, van der Zwaag W, Van de Moortele P-F, Gruetter R. MP2RAGE, a self bias-field corrected sequence for improved segmentation and T1-mapping at high field. *Neuroimage* 2010;49:1271–1281.
19. Pardoe H, Kuzniecky R. Advanced imaging techniques in the diagnosis of Nonlesional epilepsy: MRI, MRS, PET, and SPECT. *Epilepsy Curr*. 2014;14:121-124.
20. Dale AM, Fischl B, Sereno MI. Cortical surface-based analysis. I Segmentation and Surface Reconstruction. *Neuroimage*. 1999;9:179-194.
21. Thesen T, Quinn BT, Carlson C, et al. Detection of epileptogenic cortical malformations with surface-based MRI morphometry. *PloS One*. 2011;6:e16430.
22. Hutton C, De Vita E, Ashburner J, Deichmann R, Turner R. Voxel-based cortical thickness measurements in MRI. *Neuroimage* 2008;40:1701–1710.
23. Qu X, Platisa L, Despotović I, Kumcu A, Bai T, Deblaere K, Philips W. Estimating blur at the brain gray-white matter boundary for FCD detection in MRI. Conference proceedings: Annual International Conference of the IEEE Engineering in Medicine and Biology Society. IEEE Engineering in Medicine and Biology Society. Annual Conference 2014:3321–3324.
24. Weiskopf N, Suckling J, Williams G, et al. Quantitative multi-parameter mapping of R1, PD(*), MT, and R2(*) at 3T: a multi-center validation. *Front Neurosci*. 2013;7:95.
25. Widdess-Walsh P, Diehl B, Najm I. Neuroimaging of focal cortical dysplasia. *J Neuroimaging*. 2006;16:185-196.
26. Venkatesan R, Lin W, Haacke EM. Accurate determination of spin-density and T1 in the presence of RF-field inhomogeneities and flip-angle miscalibration. *Magn Reson Med*. 1998;40:592-602.

27. Wang HZ, Riederer SJ, Lee JN. Optimizing the precision in T1 relaxation estimation using limited flip angles. *Magn Reson Med*. 1987;5:399-416.
28. Preibisch C, Deichmann R. T1 mapping using spoiled FLASH-EPI hybrid sequences and varying flip angles. *Magn Reson Med*. 2009;62:240-246.
29. Volz S, Nöth U, Rotarska-Jagiela A, Deichmann R. A fast B1-mapping method for the correction and normalization of magnetization transfer ratio maps at 3 T. *Neuroimage*. 2010;49:3015-3026.
30. Yushkevich PA, Piven J, Hazlett HC, et al. User-guided 3D active contour segmentation of anatomical structures: significantly improved efficiency and reliability. *Neuroimage*. 2006;31:1116-1128.
31. Volz S, Nöth U, Deichmann R. Correction of systematic errors in quantitative proton density mapping. *Magn Reson Med*. 2012;68:74-85.
32. Geurts JJG, Roosendaal SD, Calabrese M, et al. Consensus recommendations for MS cortical lesion scoring using double inversion recovery MRI. *Neurology*. 2011;76:418-424.
33. Madhuranthakam AJ, Sarkar SN, Busse RF, Bakshi R, Alsop DC. Optimized double inversion recovery for reduction of T1 weighting in fluid-attenuated inversion recovery. *Magn Reson Med*. 2012;67:81-88.
34. Manjón JV, Thacker NA, Lull JJ, Garcia-Martí G, Martí-Bonmatí L, Robles M. Multicomponent MR Image Denoising. *Int J Biomed Imag*. 2009;2009:756897. 10 pages
35. Bouhrara M, Bonny J-M, Ashinsky BG, Maring MC, Spencer RG. Noise estimation and reduction in magnetic resonance imaging using a new multispectral nonlocal maximum-likelihood filter. *IEEE Trans Med Imaging*. 2017;36:181-193.

How to cite this article: Nöth U, Gracien R-M, Maiworm M, et al. Detection of cortical malformations using enhanced synthetic contrast images derived from quantitative T1 maps. *NMR in Biomedicine*. 2020;33:e4203. https://doi.org/10.1002/nbm.4203